Cell and tissue-specific glycosylation pathways informed by single-cell transcriptomics

Panagiotis Chrysinas[1], Shriramprasad Venkatesan[1], Isaac Ang[2], Vishnu Ghosh[1], Changyou Chen[3], Sriram Neelamegham[1,*], Rudiyanto Gunawan[1,*]

[1] Department of Chemical and Biological Engineering, University at Buffalo-SUNY, Buffalo, NY 14260

[2] Department of Computer Science, University of Illinois Urbana-Champaign, Urbana, IL 61801

[3] Department of Computer Science and Engineering, University at Buffalo-SUNY, Buffalo, NY 14260

* Co-corresponding authors: neel@buffalo.edu and rgunawan@buffalo.edu

Abstract

While single cell studies have made significant impact in various subfields of biology, they lag behind in the Glycosciences. To address this gap, we analyzed glycogene expressions in the Tabula Sapiens (TS) dataset containing ~500,000 human cells from various tissues and cell types using a recently developed glycosylation-specific gene ontology (GlycoEnzOnto). At the median sequencing (count) depth of the dataset, ~40-50 out of 400 glycogenes were detected in individual cells. Upon increasing the sequencing depth, the number of detectable glycogenes saturates at ~200 glycogenes, suggesting that the average human cell expresses ~50% of the glycogene repertoire. Hierarchies in glycogene and glycopathway expressions at single-cell level emerged from our analysis: nucleotide-sugar synthesis and transport exhibited the highest gene expressions, followed by genes for core enzymes, glycan modification and extensions, and finally terminal modifications. Notably, the same cell types showed variable glycopathway expressions based on their organ or tissue origin, suggesting nuanced, cell- and tissue-specific glycosylation patterns. Probing deeper into the transcription factors of glycogenes, we identified distinct transcriptional regulatory modules controlling terminal modifications versus other glycopathways. Finally, we developed webtools for exploring glycogene and glycopathway expressions, and transcription factors regulating glycosylation in different human cell/tissue types. Overall, the study presents an overview of glycosylation related genes and pathways across multiple human organ systems.

Introduction

Glycosylation is a ubiquitous post-translational modification that results in the formation of an array of complex carbohydrate structures or glycans in cells (Neelamegham & Mahal, 2016). These glycans, which appear either in branched or extended form on the cell surface or as single-monosaccharide additions within cells, control or fine-tune a multitude of biological functions during normal physiology and disease (Reily et al., 2019; Varki, 2017). The common glycoconjugate types on mammalian cells include: the branched N-linked glycans on glycoproteins; O-GalNAc (N-Acetyl Galactosamine) type O-glycan modifications also on glycoproteins; long repeating saccharide chains called glycosaminoglycans on a select set of proteoglycans; modifications to lipids that result in the synthesis of glycolipids; and finally O-GlcNAc (N-Acetyl Glucosamine) type single residue modifications on a broad range of nuclear proteins and transcription factors (Groth et al., 2022). Besides these major types of glycoconjugates, glycans also form the anchor for important Glycosylphosphatidylinositol (GPI)-linked cell-surface proteins. There also exist a growing list of rarer O-linked glycan modifications, including O-Glc (Glucose), O-Fuc (Fucose) and O-Man (Mannose) type glycosylation (Schjoldager et al., 2020).

Glycans on cells are formed by the concerted action of ~2% of the expressed proteome that are collectively called 'glycoEnzymes'. These enzymes are products of the corresponding 'glycogenes'. An ontology called "GlycoEnzOnto" has recently been curated to describe the existing knowledge of human glycoEnzymes within the domain of Glycosciences (Groth et al., 2022). The approximately 400 glycogenes are annotated according to their molecular functions, biological processes, and physical location (cellular component), following the Gene Ontology convention (Ashburner et al., 2000). Besides the genes encoding enzymes in the glycan biosynthesis, GlycoEnzOnto also includes the entities involved in the regulation of nucleotide-sugar metabolism, glycosyl-substrate/donor transport, glycan degradation and other regulatory components. From the molecular function perspective, glycogenes are grouped into glycosyltransferases, other transferases (e.g., sulfotransferases), modifying enzymes (e.g., epimerases and kinases), glycosidases, molecular transporters and other regulators. Additionally, glycogenes/glycoEnzymes can also be classified according to their role in glycoconjugate biosynthesis,

including: (i) The 'initiation' step that result in the attachment of the first monosaccharide or oligosaccharide to the protein/lipid; (ii) The 'elongation and branching' reactions that extend the original glycan often via lactosamine chain synthesis/branching; and (iii) The 'termination or capping' processes that prevent further chain extension. The goal of GlycoEnzOnto was to provide a shared resource that can be used for Systems Glycobiology analysis (Bennun et al., 2016; Huang et al., 2021; Kellman & Lewis, 2021; Liu & Neelamegham, 2015; Neelamegham & Liu, 2011).

This study harnesses single-cell transcriptome data of humans and the GlycoEnzOnto ontology (Groth et al., 2022) to shed light on the variation of glycopathway expression across various cell and tissue types. In particular it analyzes the Tabula Sapiens (TS) dataset that generated single-cell RNA-sequencing (scRNA-seq) data for 483,152 human cells from 15 donors which had been organized into 24 tissues and over 400 cell types (Tabula Sapiens et al., 2022). Such single-cell data identify subtle, yet potentially vital, differences in glycosylation processes among different cells within the same tissue or organ as this is not possible using bulk sequencing. Our results show that only 50% of glycogenes are expressed in a given cell, with expression levels varying depending on gene function. In contrast to conventional thinking based on microarray/quantitative-PCR data analysis (Nairn et al., 2008) that suggests that glycogenes are lowly expressed, our more holistic single-cell analysis reveals that the glycogenes are expressed at levels that are comparable to other protein-coding genes. Further, our analysis presents a map of glycopathway expression across tissue, illustrating the inherent heterogeneity across human cells and tissues. Specifically, the findings showed how enzymes involved in the metabolism of nucleotide sugars, glycan degradation processes, and biosynthesis of core structures, exhibit uniform and ubiquitous expression patterns across cell types and tissues, consistent with their foundational roles in glycan biosynthesis. Meanwhile, terminal glycoenzymes often serve specialized roles, and they are more selectively expressed in individual cell types. The analysis of transcriptional factors in the TS dataset using normalized mutual information of TF-glycogene expression reveals two transcriptional regulatory modules (TRMs), with one module controlling terminal glycan modifications and a second regulating other glycopathways. To bolster the accessibility, we also developed webtools that allow further exploration of glycogenes, glycopathways and related transcription factors at single cell level (www.virtualglycome.org/glycoCARTA/ and www.virtualglycome.org/glycoTF).

Results

Overview of glycogene expression in single cell studies

Single-cell RNA-sequencing (scRNA-seq) technologies are transforming our understanding of cell biology, from development (Farrell et al., 2018; Griffiths et al., 2018) to immune systems (Ginhoux et al., 2022; Tian et al., 2022) and to aging (Perez et al., 2022; Tabula Muris, 2020). While different single-cell methods have their advantages and disadvantages, they share a few issues, such as low mRNA capture efficiency and high dropout rates, that particularly affect the measurement of genes with low expression (Jiang et al., 2022; Luecken & Theis, 2019). As glycogenes are traditionally thought to be lowly expressed (Nairn et al., 2008), this study assessed the ability of single-cell data to inform us about genes and pathways involved in glycosylation by analyzing scRNA-seq data from the Tabula Sapiens (TS) project.

We applied the bioinformatics analysis workflow depicted in **Fig. 1A** to the TS dataset, focusing on glycogenes and glycopathways presented in GlycoEnzOnto (Groth et al., 2022). We compared the

expression profiles of 400 glycogenes to 19,447 protein coding (PC) genes in the TS dataset (**Suppl. Table S1)**. As expected, the number of detectable glycogenes in the TS cells increased with the cell's UMI count depth (**Fig. 1B**). Specifically, at the median (mean) UMI count depth of 6496 (10181) we detected between 2 and 98 glycogenes (2 to 118 genes) with RNA count > 0 and a median value of 40 glycogenes/cell (a mean value of 58 glycogenes/cell). Thus, only 10% of all glycogenes are detected in the median cell in the TS dataset (or 14.5% of glycogenes for the mean cell). The low level of detection of glycogenes (*i.e.*, 10-14.5%) might stem from the overall low expression of glycogenes. Increasing the UMI count depth did enhance glycogene detectability. However, the maximum number of captured glycogenes reached a plateau at around 220, suggesting that, at most, only 50-60% of all glycogenes are expressed in individual cells. Lastly, only a marginal improvement in the number of detected glycogenes was observed beyond ~65,000 UMI counts per cell, at which point about 165 glycogenes (median) were detected (**Fig. 1B**).

We observed a strong correlation between the number of glycogenes and the number for other PC genes detected in cells (**Fig. 1C**). Comparing the distribution of expression between glycogenes and other PC genes, using the fraction of expressing cells as an indicator of gene expression level, revealed a significant difference between the two groups (*p*-value = 1.19×10^{-7}, Kolmogorov-Smirnov test) (see **Methods** and **Fig. 1D**). Interestingly, in the TS cells, glycogenes were more commonly expressed than other PC genes (p-value = 5.33×10^{-5}, two-sided Wilcoxon ranksum test). But, despite this prevalence, glycogenes were not among the highly expressed genes in the TS dataset (**Fig. 1D** inset)—in fact, glycogenes were depleted among the top 10% of highest expressing PC genes (odds ratio = 0.655, p-value = 0.03, two-sided Fisher exact test). Overall, the data suggested that while the glycogenes may not be among the most highly expressed genes, they are more ubiquitously expressed, frequently at levels comparable to or higher than the average PC gene.

Variability in glycogene expression patterns across cell types and tissues

We delved deeper into the variability of glycogene expression among functional sub-groups using the GlycoEnzOnto as a guide. To do this, we evaluated the fraction of cells expressing glycogenes across different sub-groups (**Suppl. Tables S2 and S3**). **Fig. 1E** reveals that glycogenes belonging to the 'Transporters and Regulators' sub-groups—that is, genes involved in the creation of nucleotide-sugars, monosaccharide transport and related metabolism—generally exhibited higher expression than other glycogene sub-groups. Glycogenes responsible for glycan modifications and those producing glycosidases displayed comparable expression levels with both gene groups presenting moderate expression. Finally, the glycotransferases and other transferases demonstrated the lowest expression levels. Delving further into glycogenes associated with the biosynthesis of core structures (Core), glycan chain elongation (Extension), and capping of glycan structures (Terminal), the Core and Extension groups showed similar levels of expression that were higher than the expression of glycogenes in the Terminal group (**Fig. 1F**). These patterns align with the role of the core enzymes in initiating the formation of specific glycan types, except perhaps for the case of O-GalNAc type carbohydrate chain formation that can be catalyzed by various isoenzymes. Thus, these Core genes are more broadly expressed in various cells compared to terminal modifiers that are expressed in a tissue specific manner (Dworkin et al., 2022). Although our analysis employed the fraction of expressing cells as the metric for gene expression level—following the recommendation for lowly expressed genes (Booeshaghi & Pachter, 2021)—we observed similar trends using the mean expression of genes across cells (see **Suppl. Fig. S1**).

Next, we investigated how glycogene expression pattern in individual cells varies across different cell types and tissue types using scVI (single-cell Variational Inference) for latent embedding and UMAP (Unified Manifold Approximation and Projection) for 2D visualization (**Fig. 1G** and **H**, and **Suppl. Fig. S2**). Examining epithelial cells (**Fig. 1G**), a natural clustering (grouping) of cells emerged in the UMAP plot following their tissue sources. Interestingly, even for cells from the same tissue, for example liver, pancreas and salivary gland, distinct cell groupings appeared. We made similar observations for endothelial, stromal and immune cells in the TS dataset (see **Supplementary Figure S2A-B**). Shifting focus to cells in the blood tissue (**Fig. 1H** and **Fig. S2D**), these cells formed clusters according to their lineage along the hematopoietic stem cell (HSC) differentiation pathway. Specifically, cells from the lymphoid path, including B cell, T cells, Natural Killer (NK) T cell, and plasma cells, appeared in overlapping clusters, while cells from the granulocyte-macrophage lineage, including macrophages, monocytes, and neutrophils, formed separate groups. The overt grouping of cells, influenced by their tissue of origin and lineage, suggests that mammalian tissues and cell types possess unique single-cell glycogene expression patterns, potentially indicating their varied glycan structures. Still, we caution that such 2D UMAP plots may distort cell-cell similarities in single-cell gene expression (Chari & Pachter, 2023; Wang et al., 2023). In subsequent analyses, we employed the glycogene expression directly, rather than using UMAP latent embeddings.

Glycopathway expression vary with tissue and cell type of origin

A rich diversity of glycan structures arises from sets of reactions operating together as "glycopathways". To gauge the expression of these glycopathways in TS cells, we calculated the expression of glycopathways in the TS cells by taking the average expression of the genes from each glycopathway as delineated in the GlycoEnzOnto (see **Suppl. Table S3**). To further discern the patterns of glycopathway expressions, differential expression (DE) analysis was performed (**Fig. 2**). As illustrated in **Fig. 2A**, the DE analysis combined two information: zero-inflated mean expression of glycopathways for cells in each tissue type; and log-fold change (logFC) of the glycopathway mean expression value in a given tissue against cells in all other tissues. The intensity of green color in the DE heatmap plot informs the glycopathway expression while the border thickness indicates the logFC. In the example of enzymes involved in extension of the glycolipid (GSL) core and its diversification into ganglio-, lacto-, neolacto- and globo-series (**Fig. 2A**), we found a higher expression of relevant genes in eyes, trachea and small intestines compared to other tissues.

Fig. 2B visualizes the mean and differential expression of various glycopathways across epithelial cells found in multiple tissue-types. Here, glycopathways are grouped into three major functional categories: Core, Extension, and Terminal pathways (Groth et al., 2022). The results for three additional glycopathway groups: Core subclass, Nucleotide sugar (NS) metabolism, and Degradation processes are provided in **Suppl. Fig S3A**. The same analyses are also performed for Endothelial, Stromal and Immune cell types, and the results are presented in **Suppl. Fig. S4A-S6A**. **Suppl. Table 4** provides the mean expressions of the glycopathways for the cell types in the TS dataset. The color scale bar for mean expression used in Fig. 2 and the aforementioned supplemental figures is the same, allowing direct comparison between the cell/tissue types. Additionally, the observations are independent of cell sample size since the mean expression of glycogenes in a system did not depend on either the number of cells in the tissues ($\rho = -0.22$, p-value = 0.30) or the number of cells of a given population ($\rho = -0.15$, p-value = 0.81).

The data present several striking observations. Notably, endothelial and stromal cells consistently manifested higher levels of glycopathway expression in comparison to epithelial and immune cells. Surveying the groups of glycopathways, the Core, NS metabolism, and Degradation groups had the highest

mean glycogene expressions. These observations are in agreement with the expression analysis of glycogenes from these pathways in **Fig. 1E** and **1F**. The trend also underscores the broad functions that these groups of glycopathways have in terms of controlling global glycan turnover rates and pathway initiation steps. In general, the most highly expressed core gene set across all cell/tissue type belonged to the O-GlcNAc forming enzymes OGT and OGA. This highlights the importance of O-GlcNAc post-translational modification in regulating a broad swath of cellular signaling, transcription and disease processes (Hart et al., 2011). Besides these enzymes, we also observed consistent high expressions of several other core-pathways in diverse cell types, particularly those initiating GSL biosynthesis (*i.e.*, 'GlcCer-series') and those initiating the synthesis of N-linked glycans (*i.e.*, 'Dolichol pathways'). In addition to the core Dolichol pathway, high gene expression was also observed for N-glycosylation processing enzymes that trim the initial dolichol precursor to enable protein folding and the biosynthesis of complex type structures. Finally, the prevalence of core-3 and core-4 O-GalNAc biosynthetic genes were largely restricted to the intestines, and this too is consistent with literature knowledge (Brockhausen, 2006; Yang et al., 1994).

Glycosaminoglycans were expressed in stromal cells, particularly with respect to hyaluronan forming enzymes (HAS1, HAS2, HAS3) which were consistently high in fibroblasts and connective tissue in multiple organs. Among the rarer O-linked glycan modifications, enzyme contributing to O-mannosylation of cadherin superfamily (Larsen et al., 2019), particularly TMTC1 was highly expressed in vascular endothelial cells (**Fig. S4A**). Not much is known about these pathways, but the measured high gene expression warrants additional investigation regarding its biological function. Among the enzymes involved in nucleotide biosynthesis, we noted high levels of UGDH (UDPGlcA_synth) and UXS1 (UDPXyl_synth) which are involved in the biosynthesis of starting materials that contribute to glycosaminoglycan biosynthesis. Enzymes in the biosynthesis of other nucleotide-sugar donors were also present in all cells, albeit at lower levels. Finally, several enzymes involved in lysosomal targeting and trafficking (lyso_target) of glycosidases were also highly expressed (**Suppl. Table. S4**).

Among the enzymes mediating glycan extension, high expressions were noted in pathways involved in the biosynthesis of Type-II lactosamine (Galβ1-4GlcNAcβ) and Type-III lactosamine (Galβ1-3GalNAcβ) chains across all cell and tissue-types, compared to Type-I lactosamine (Galβ1-3GlcNAcβ) chains. This is generally consistent with current biological knowledge related to the high abundance of Type-II lactosamine chains on N-/O-linked glycans and GSLs. Interestingly, the abundance of I-branching enzymes GCNT2 and 3 were restricted to specific tissue types supporting the emerging notion that such GlcNAcβ1-6 branching may have important biological functions for example in regulating cell growth and survival (Colosimo et al., 1991). Additional extension glycopathways that were highly expressed were involved in the N-glycosylation processing enzymes that are expressed in the endoplasmic reticulum (Ngly_trim) and the keratan sulfate extension enzymes (KS_poly). The epithelial cells of the liver, which is a major source of heparan sulfate biosynthesis, also had expression of HS extension genes at high levels.

The expression levels of chain terminating enzymes were often low and heterogenous, across cell-types. The only exception to this were the enzymes involved in protein tyrosine sulfonation (TyrP-synth) which were uniformly expressed at high levels in all cells and tissues. This is consistent with the ubiquitous nature this modification. Genes related to ABO antigen had the highest expression in epithelial cells (see **Suppl. Table. S4**) as these cells are a major source of blood group antigens. Finally, among the lowly expressed glycopathways, SDA antigen (Sda) biosynthetic enzymes were restricted to epithelial and immune cells while the enzymes forming sialyl Lewis-X epitope were dominant in T-cells, monocytes and neutrophil populations based on expression of the enzyme FUT7.

The logFCs for glycopathway expression are generally moderate, ranging from –0.81 to 1.37, suggesting the prevalence of similar pathways in different cell types. Among the pathways, Core and Extension groups display greater logFC magnitudes than those in the Terminal group suggesting heightened tissue-to-tissue variability. Similar to the Terminal group, the Core subclass, together with the NS and Degradation groups, exhibits only modest logFCs across different tissues. Upon examining individual tissues, cells in the eye, heart, and lung typically demonstrated higher overall glycopathway expressions when compared to other cells. In contrast, cells in the kidney and liver display relatively lower overall expressions. Interestingly, cells originating from tissues that are related to each other, such as large and small intestines, present similar expression patterns as shown by hierarchical clustering in **Fig. 2** and **Suppl. Fig. S3**. Overall, several of our computational predictions are consistent with literature and our analysis also suggest additional hypothesis that will need additional experimental validation. To facilitate such comprehensive exploration of glycopathways, we have developed a webtool that is accessible via: http://www.virtualglycome.org/glycoCARTA/.

Glycopathway expression vary with tissue and cell type of origin

While DE analysis focuses on differences in the mean expression, we complemented this with enrichment/depletion (ED) analysis. This analysis determines if a specific tissue are disproportionately enriched or depleted of cells that are expressing a given glycopathway—termed as "expressing cells"—when compared to the overall proportion of expressing cells in the entire TS dataset. Given that a number of glycopathways demonstrated low single-cell expressions, the fraction of expressing cells has been proposed as a better metric for gauging expression within a cell population (Booeshaghi & Pachter, 2021). To this end, for every combination of glycopathway and tissue, we constructed a contingency table showing the count distribution of expressing/non-expressing cells for the glycopathway and of cells from/outside of the tissue (**Fig. 3A**, see Methods). Utilizing this table, we evaluated the log2 odds ratio (logOR). A logOR greater or lesser than 0 suggests that the particular tissue contains more or fewer expressing cells than expected based on the overall proportion of expressing cells in the TS dataset. In effect, a positive (negative) logOR indicates enrichment (depletion) of cells expressing the designated glycopathway in that tissue.

The results of the ED analysis as shown in **Fig. 3B** resonated well with the DE analysis findings. With the exception of the GalCer pathway in the kidney, pathways with positive (negative) logOR generally had positive (negative) log2FC. Also, there was a positive correlation between the logORs and the logFC (Pearson correlation $\rho = 0.61$). In summary, the results of both DE and ED analysis highlight a moderate variability in glycopathway expressions across tissues, especially in the Core and Extension groups. Conversely, the Terminal, Core subclass, Nucleotide sugar and Degradation manifest higher variation in single-cell expression across different tissues. Additional wet-lab studies are warranted to determine how the variation in gene expression across tissue relate to tissue-specific glycan structure patterns.

Transcriptional factors of glycosylation extracted from single-cell RNA-seq

Literature reported experimentally validated transcription factors (TFs) regulating glycogenes are few (Groth et al., 2022). To address this gap, we leveraged single cell transcriptomics data in the TS and the TF-gene binding interaction data in TFLink database (Liska et al., 2022). Our strategy involved evaluating normalized mutual information (NMI) of single-cell gene expression between every possible pair of transcription factor (TF) and glycogene. Here, mutual information (MI) gives a measure of how much uncertainty in the expression of a glycogene is reduced given the corresponding expression data for a TF.

As the value of this MI depends on the gene expression entropy of the TF and glycogene, we normalized the MI by the minimum between the two entropies. Applying this strategy, the NMI yielded an accurate prediction for TF-glycogene interactions, achieving an Area under Precision-Recall Curve (AUPRC) of 0.45, when compared to binding interactions sourced from the TFLinks (Liska et al., 2022). This accuracy outperformed both the pairwise Pearson correlation (AUPRC = 0.40) and the Spearman rank correlation (AUPRC = 0.40). Still, all of the above interaction metrics: NMI, Pearson correlation, and Spearman rank correlation, surpassed a random predictor (AUPRC = 0.31). This outcome suggests that single-cell gene expression data may be used to improve TF-glycogene interaction predictions.

Our single-cell TF-glycogene evaluation enables the identification of transcriptional regulatory modules (TRMs) of glycosylation, specifically by clustering glycogenes based on the similarities of their NMIs. Here, a TRM is a set of genes whose transcription is regulated by a shared regulatory program (Segal et al., 2003). For this purpose, we first filtered the TFs to include only those that have NMIs larger than the 95th percentile for each glycogene. Hierarchical clustering and silhouette analysis for *k*-means clustering as shown in **Fig. 4A-B** suggest two TRMs in the TS dataset. Correspondingly, we performed *k*-means clustering using $k = 2$, followed by Fisher's exact test with Bonferroni correction ($\alpha = 0.05$) to relate each cluster with glycopathways. Interestingly, as depicted in **Fig. 4C** (see also **Suppl. Fig. S7**), the first TRM (Cluster 0) is strongly associated with the Terminal group, while the other (Cluster 1) is connected to Core subclass and Nucleotide sugar groups. For the second TRM, we also noted over-representations (odd ratio > 1) of Core and Degradation glycopathways, but the association was not statistically significant at $\alpha = 0.05$. These results above suggest that Terminal glycopathways are under a distinct regulatory program, fully consistent with the overt differences in the DE and ED analysis results between Terminal and other glycopathways. The shared and distinct TFs associated with these TRMs are presented in **Suppl. Table S5**.

For exploration of the complete TF-glycogene analysis using NMI, we created the following website: www.virtualglycome.org/glycoTF.

Discussion

A key contribution from this study is the elucidation of the broad landscape of glycopathway expressions across human cell types and tissues. The findings are in broad agreement with the recent work by Joshi and colleagues (Dworkin et al., 2022) that showed that core enzymes are more ubiquitously expressed among cells than enzymes that modify terminal glycan residues which cater to more specialized functions. However, it is important to note differences in the study design as the glycogene set used in this work is considerably larger (224 in Joshi vs. 400 in this work), owing to the inclusion of glycosidases, transporters and other regulators of carbohydrate biosynthesis. In addition, the focus on glycopathways in our study represents another important deviation from the previous study. The approach taken in this study is also distinct in that single-cell gene expression data are used directly without pseudobulking. The use of differential expression (DE) and enrichment-depletion (ED) analysis, as opposed to using inter-quartile distances to judge the importance of specific glycogenes, is another difference. Lastly, the inference of TF-glycogene analysis using single-cell gene expression data via normalized mutual information is unique to our study. As demonstrated, such analysis enables elucidation of transcriptional regulatory modules of glycosylation.

Yet, while our study represents a broad analysis for understanding glycosylation in humans, it is not without limitations. At the sequencing depth employed in the TS, out of the anticipated ~220 glycogenes expressed human cells, less than one fifth are detected in a typical cell in this dataset. While this low detection is comparable with other PC genes, such high data sparsity impedes data analysis such

as single-cell clustering. Besides, the TS data does not include key organs like the brain which have distinct glycosylation profiles compared to other organs. Additional data analysis is thus required to integrate the findings of this work with brain initiatives and related activities (Ament et al., 2023). In addition, while our analysis captures the nuances of gene expression patterns related to glycosylation, extrapolating these findings to the functional outcomes, specifically the glycosylation structure and function, is required in the future. Such an endeavor requires the development of novel technologies to measure glycoenzyme activity and parallel analysis of the glycome at single cell level. Further, such development will require us to understand the details of a myriad of steps (transcription, translation, biosynthetic reactions) each of which influence the functional outcome of cells. Due to these complexities, the observed variations in gene expression described in this manuscript may only describe a portion of cellular variations in glycome. Direct validation, such as through glycomics analysis at single-cell level and CRISPR technology based molecular screens, would be paramount in solidifying our inferences and bridging the gap between gene expression and functional glycan structures on proteins.

Methods

Tabula Sapiens data preprocessing

The scRNA-seq data in the Tabula Sapiens (TS) project were generated using two different single-cell sequencing technologies: 10X and Smart-seq, with the majority of the data coming from 10X (456,101 cells vs. 27,051 cells). Tabula Sapiens scRNA-seq data were obtained from the public website (Consortium, 2022). This study focused only on scRNA-seq data from 10X platform to avoid any potential batch effects associated with different sequencing platforms.

The data preprocessing is illustrated in **Fig. 1A,** with individual steps being carried out using the Python package `scanpy` (Wolf et al., 2018). The analysis started with the decontaminated UMI counts from the TS dataset. Decontamination of background RNA was previously performed using the method decontX (Yang et al., 2020). Following the standard practice, UMI counts were scaled cellwise so that each cell has a count depth of 10,000. This scaling produced relative RNA abundances x_i that are comparable across cells.

For differential expression analysis, the scaled UMI counts were log-transformed (*i.e.*, $\log(x_i + 1)$) to satisfy the input requirement of the method MAST (Finak et al., 2015). For subsequent analyses, we subset the preprocessed count matrix to 19,847 transcripts (from a total of 58,559) associated with protein-coding (PC) genes as defined in BioMart. On average, PC genes make up 89.4% of the total number of reads. Out of these, we extracted data for 400 glycosylation-related genes (glycogenes) as defined in the GlycoEnzOnto (Groth et al., 2022). Python and R codes used for data analysis are available at: http://www.github.com/cabselab/glyTS .

scVI+UMAP embedding

To visualize glycogene expression in single cells, Single-cell Variational inference (scVI) was applied to the decontaminated glycogene UMI counts to generate a lower dimensional embedding of the glycogene expression (Lopez et al., 2018). The method scVI produces a probabilistic latent space of single-cell gene expression data based on zero-inflated negative binomial distribution. Specifically, the Python's `scvi-tools` package (Gayoso et al., 2022) was implemented with the following parameters: $n_{latent} = 50$, n_{layers}

= 3, n_{latent} = 50, and dropout rate = 50. For this study, only the variational posterior of the scVI model was employed. For visualization of this embedding, a Uniform Manifold Approximation and Projection (UMAP) using $n_{neighbors}$ = 15 and $n_{components}$ = 2 (2D) was used (McInnes et al., 2018).

Differential expression analysis of glycopathways

Glycosylation-related pathways (glycopathways) are described in **Suppl. Table S3**. DE analysis using MAST requires as inputs the $\log(x_i + 1)$-transformed UMI counts for the glycogene expression. For each pathway, its expression was evaluated by averaging the expression of glycogenes belonging to that pathway. Differential expression (DE) analysis of glycopathways was then performed using the MAST (Model-based Analysis of Single cell Transcriptomics). MAST adapts a hurdle model to tackle zero-inflation and biomodality of single-cell transcriptome data (Finak et al., 2015). As illustrated in **Fig. 2A**, MAST produces fold-change differences of the mean expression of a glycopathway between cells from a specific tissue, with respect to all other tissue with the same glycopathway. Associated statistical significance is also calculated. The DE analysis was implemented using the Seurat package (version 4.1.0) in R, specifically `FindAllMarkers` routine (Hao et al., 2021).

Glycopathway enrichment analysis in tissues

Enrichment analysis was performed to assess whether cells from a specific tissue are over-represented or depleted with cells expressing a given glycopathway. Here, a cell is labeled as an "expressing cell" when the average expression (scaled UMI count) of genes in a glycopathway is nonzero. For a given pair of glycopathway and tissue, a contingency table was constructed to distribute the cells into two distinct categorizations: expressing cells / non-expressing cells and cells in the tissue / cells not in the tissue, as follow:

	Expressing cells	Non-expressing cells
Cells in tissue	a	b
Cells not in tissue	c	d

The odds ratio OR, given by ad/bc, indicates the overrepresentation (odds ratio > 1 or log(OR) > 0) or depletion (odds ratio < 1 or log(OR) < 0) of expressing cells in a tissue. The statistical significance was established via Fisher's exact test based on hypergeometric sampling. The enrichment analysis was implemented in Python using fisher_exact routine from the `scipy` package (version 1.10.1).

Transcriptional factor-glycogene analysis

The curation of TF-glycogene and glycopathway interactions involved evaluating normalized mutual information (MI) of single-cell expression between every possible pair of TF-glycogene in the TFLink database (Liska et al., 2022). TF-gene interactions in the TFLink database were originally compiled from numerous databases that relied on different evidence of TF binding on the regulatory elements of the genes (Liska et al., 2022). Here, normalized MI was used to provide additional evidence for TF-glycogene

interactions based on shared information in their single-cell expression. The following equation gives the basis for evaluating MI for TF-glycogene relations:

$$I(TF,G) = \sum_{t_i=0}^{10^4} \sum_{g_j=0}^{10^4} P_{(TF,G)}(tf,g) log \frac{P_{(TF,G)}(tf,g)}{P_{TF}(tf)P_G(g)}$$

where $P_{(TF,G)}$ denotes the joint probability distribution of single-cell expression of a transcription factor TF and a glycogene G, and P_{TF} and P_G denote the marginal probability distribution of TF and G, respectively. We evaluated $I(TF,G)$ using the scaled UMI counts from all 10X cells in the TS dataset.

Since the MI for a given TF-gene pair depends on the distribution entropy (uncertainty) in both the TF and the gene, normalized MI was used to enable comparison across TFs and genes. The normalized MI (I_{norm}) was evaluated as follows:

$$I_{norm}(TF,G) = \frac{I(TF,G)}{\min\left(H_{TF}(TF), H_G(G)\right)}$$

where the Shannon entropies for the TF and glycogene, denoted above as H_{TF} and H_G, respectively, were computed based on the following equations:

$$H_{TF}(TF) = -\sum_{t_i=0}^{10^4} P_{TF}(tf) log P_{TF}(tf)$$

$$H_G(G) = -\sum_{g_i=0}^{10^4} P_G(g) log P_G(g)$$

The calculation of MI and Shannon entropy were performed using the Python package `sklearn` (Pedregosa et al., 2011). Finally, TF-glycogene interactions were trimmed, where for each gene, only the highest 5th percentile of TFs in terms of normalized MI were kept. Then, for each glycopathway, the union of TFs from all genes in the pathway was taken to provide TF-glycopathway interactions.

Transcriptional regulatory module analysis

Transcriptional regulatory modules were identified by clustering glycogenes based on the logarithm of NMIs. The list of TFs were first filtered to keep only those with NMIs larger than the 95th percentile for each glycogene. Silhouette analysis was performed by computing silhouette scores for different runs of *k*-means clustering for a range of *k* (*k* = 1 to 15). The silhouette score is a value between –1 and 1, where 1 is considered the ideal clustering result (Rousseeuw, 1987). Each glycogene cluster was taken as a transcriptional regulatory module. Enrichment analysis was performed using the Fisher's exact test to identify the over-representation of glycopathways. For this purpose, we employed the glycopathway definition given in **Suppl. Table S3**. Given two sets of glycogenes, one from a TRM and another from a glycopathway, we constructed the following contingency table:

	Glycogenes in Pathway	Glycogenes not in Pathway
Glycogenes in TRM	m	n
Glycogenes not in TRM	s	t

The odds ratio calculation ($OR = mt/ns$) and Fisher's exact test were performed following the same procedure for the ED analysis (see **Glycopathway enrichment analysis in tissues**). Hierarchical and *k*-means clustering were implemented using the `scikit-learn` package (version 1.2.2) and the Fisher's exact test using the `scipy` package (version 1.10.1) in Python.

References

Tabula Sapiens, C., Jones, R. C., Karkanias, J., Krasnow, M. A., Pisco, A. O., Quake, S. R., . . . Wyss-Coray, T. (2022). The Tabula Sapiens: A multiple-organ, single-cell transcriptomic atlas of humans. *Science, 376*(6594), eabl4896. doi:10.1126/science.abl4896

Ament, S. A., Adkins, R. S., Carter, R., Chrysostomou, E., Colantuoni, C., Crabtree, J., Creasy, H. H., Degatano, K., Felix, V., Gandt, P., Garden, G. A., Giglio, M., Herb, B. R., Khajouei, F., Kiernan, E., McCracken, C., McDaniel, K., Nadendla, S., Nickel, L., . . . White, O. R. (2023). The Neuroscience Multi-Omic Archive: a BRAIN Initiative resource for single-cell transcriptomic and epigenomic data from the mammalian brain. *Nucleic Acids Res*, *51*(D1), D1075-D1085. https://doi.org/10.1093/nar/gkac962

Ashburner, M., Ball, C. A., Blake, J. A., Botstein, D., Butler, H., Cherry, J. M., Davis, A. P., Dolinski, K., Dwight, S. S., Eppig, J. T., Harris, M. A., Hill, D. P., Issel-Tarver, L., Kasarskis, A., Lewis, S., Matese, J. C., Richardson, J. E., Ringwald, M., Rubin, G. M., & Sherlock, G. (2000). Gene ontology: tool for the unification of biology. The Gene Ontology Consortium. *Nat Genet*, *25*(1), 25-29. https://doi.org/10.1038/75556

Bennun, S. V., Hizal, D. B., Heffner, K., Can, O., Zhang, H., & Betenbaugh, M. J. (2016). Systems Glycobiology: Integrating Glycogenomics, Glycoproteomics, Glycomics, and Other 'Omics Data Sets to Characterize Cellular Glycosylation Processes. *J Mol Biol*, *428*(16), 3337-3352. https://doi.org/10.1016/j.jmb.2016.07.005

Booeshaghi, A. S., & Pachter, L. (2021). Normalization of single-cell RNA-seq counts by log(x + 1)dagger or log(1 + x)dagger. *Bioinformatics*, *37*(15), 2223-2224. https://doi.org/10.1093/bioinformatics/btab085

Brockhausen, I. (2006). Mucin-type O-glycans in human colon and breast cancer: glycodynamics and functions. *EMBO Rep*, *7*(6), 599-604. https://doi.org/10.1038/sj.embor.7400705

Chari, T., & Pachter, L. (2023). The specious art of single-cell genomics. *PLoS Comput Biol*, *19*(8), e1011288. https://doi.org/10.1371/journal.pcbi.1011288

Colosimo, C., Rossi, P., Elia, M., Bentivoglio, A. R., Altavista, M. C., & Albanese, A. (1991). Transient alternating hemichorea as presenting sign of progressive supranuclear palsy. *Ital J Neurol Sci*, *12*(1), 99-101. https://doi.org/10.1007/BF02337621

Consortium, T. S. (2022). *Tabula Sapiens Portal*. https://tabula-sapiens-portal.ds.czbiohub.org/

Dworkin, L. A., Clausen, H., & Joshi, H. J. (2022). Applying transcriptomics to studyglycosylation at the cell type level. *iScience*, *25*(6), 104419. https://doi.org/10.1016/j.isci.2022.104419

Farrell, J. A., Wang, Y., Riesenfeld, S. J., Shekhar, K., Regev, A., & Schier, A. F. (2018). Single-cell reconstruction of developmental trajectories during zebrafish embryogenesis. *Science*, *360*(6392). https://doi.org/10.1126/science.aar3131

Finak, G., McDavid, A., Yajima, M., Deng, J., Gersuk, V., Shalek, A. K., Slichter, C. K., Miller, H. W., McElrath, M. J., Prlic, M., Linsley, P. S., & Gottardo, R. (2015). MAST: a flexible statistical framework for assessing transcriptional changes and characterizing heterogeneity in single-cell RNA sequencing data. *Genome Biol*, *16*, 278. https://doi.org/10.1186/s13059-015-0844-5

Gayoso, A., Lopez, R., Xing, G., Boyeau, P., Valiollah Pour Amiri, V., Hong, J., Wu, K., Jayasuriya, M., Mehlman, E., Langevin, M., Liu, Y., Samaran, J., Misrachi, G., Nazaret, A., Clivio, O., Xu, C., Ashuach, T., Gabitto, M., Lotfollahi, M., . . . Yosef, N. (2022). A Python library for probabilistic analysis of single-cell omics data. *Nat Biotechnol*, *40*(2), 163-166. https://doi.org/10.1038/s41587-021-01206-w

Ginhoux, F., Yalin, A., Dutertre, C. A., & Amit, I. (2022). Single-cell immunology: Past, present, and future. *Immunity*, *55*(3), 393-404. https://doi.org/10.1016/j.immuni.2022.02.006

Griffiths, J. A., Scialdone, A., & Marioni, J. C. (2018). Using single-cell genomics to understand developmental processes and cell fate decisions. *Mol Syst Biol*, *14*(4), e8046. https://doi.org/10.15252/msb.20178046

Groth, T., Diehl, A. D., Gunawan, R., & Neelamegham, S. (2022). GlycoEnzOnto: a GlycoEnzyme pathway and molecular function ontology. *Bioinformatics*, *38*(24), 5413-5420. https://doi.org/10.1093/bioinformatics/btac704

Hao, Y., Hao, S., Andersen-Nissen, E., Mauck, W. M., 3rd, Zheng, S., Butler, A., Lee, M. J., Wilk, A. J., Darby, C., Zager, M., Hoffman, P., Stoeckius, M., Papalexi, E., Mimitou, E. P., Jain, J., Srivastava, A., Stuart, T., Fleming, L. M., Yeung, B., . . . Satija, R. (2021). Integrated analysis of multimodal single-cell data. *Cell*, *184*(13), 3573-3587 e3529. https://doi.org/10.1016/j.cell.2021.04.048

Hart, G. W., Slawson, C., Ramirez-Correa, G., & Lagerlof, O. (2011). Cross talk between O-GlcNAcylation and phosphorylation: roles in signaling, transcription, and chronic disease. *Annu Rev Biochem*, *80*, 825-858. https://doi.org/10.1146/annurev-biochem-060608-102511

Huang, Y. F., Aoki, K., Akase, S., Ishihara, M., Liu, Y. S., Yang, G., Kizuka, Y., Mizumoto, S., Tiemeyer, M., Gao, X. D., Aoki-Kinoshita, K. F., & Fujita, M. (2021). Global mapping of glycosylation pathways in human-derived cells. *Dev Cell*, *56*(8), 1195-1209 e1197. https://doi.org/10.1016/j.devcel.2021.02.023

Jiang, R., Sun, T., Song, D., & Li, J. J. (2022). Statistics or biology: the zero-inflation controversy about scRNA-seq data. *Genome Biol*, *23*(1), 31. https://doi.org/10.1186/s13059-022-02601-5

Kellman, B. P., & Lewis, N. E. (2021). Big-Data Glycomics: Tools to Connect Glycan Biosynthesis to Extracellular Communication. *Trends Biochem Sci*, *46*(4), 284-300. https://doi.org/10.1016/j.tibs.2020.10.004

Larsen, I. S. B., Narimatsu, Y., Clausen, H., Joshi, H. J., & Halim, A. (2019). Multiple distinct O-Mannosylation pathways in eukaryotes. *Curr Opin Struct Biol*, *56*, 171-178. https://doi.org/10.1016/j.sbi.2019.03.003

Liska, O., Bohar, B., Hidas, A., Korcsmaros, T., Papp, B., Fazekas, D., & Ari, E. (2022). TFLink: an integrated gateway to access transcription factor-target gene interactions for multiple species. *Database (Oxford)*, *2022*. https://doi.org/10.1093/database/baac083

Liu, G., & Neelamegham, S. (2015). Integration of systems glycobiology with bioinformatics toolboxes, glycoinformatics resources, and glycoproteomics data. *Wiley Interdiscip Rev Syst Biol Med*, *7*(4), 163-181. https://doi.org/10.1002/wsbm.1296

Lopez, R., Regier, J., Cole, M. B., Jordan, M. I., & Yosef, N. (2018). Deep generative modeling for single-cell transcriptomics. *Nat Methods*, *15*(12), 1053-1058. https://doi.org/10.1038/s41592-018-0229-2

Luecken, M. D., & Theis, F. J. (2019). Current best practices in single-cell RNA-seq analysis: a tutorial. *Mol Syst Biol*, *15*(6), e8746. https://doi.org/10.15252/msb.20188746

McInnes, L., Healy, J., Saul, N., & Großberger, L. (2018). UMAP: Uniform Manifold Approximation and Projection. *Journal of Open Source Software*, *3*(29), 861. https://doi.org/10.21105/joss.00861

Nairn, A. V., York, W. S., Harris, K., Hall, E. M., Pierce, J. M., & Moremen, K. W. (2008). Regulation of glycan structures in animal tissues: transcript profiling of glycan-related genes. *J Biol Chem*, *283*(25), 17298-17313. https://doi.org/10.1074/jbc.M801964200

Neelamegham, S., & Liu, G. (2011). Systems glycobiology: biochemical reaction networks regulating glycan structure and function. *Glycobiology*, *21*(12), 1541-1553. https://doi.org/10.1093/glycob/cwr036

Neelamegham, S., & Mahal, L. K. (2016). Multi-level regulation of cellular glycosylation: from genes to transcript to enzyme to structure. *Curr Opin Struct Biol*, *40*, 145-152. https://doi.org/10.1016/j.sbi.2016.09.013

Pedregosa, F., Varoquaux, G., Gramfort, A., Michel, V., Thirion, B., Grisel, O., Blondel, M., Prettenhofer, P., Weiss, R., Dubourg, V., Vanderplas, J., Passos, A., Cournapeau, D., Brucher, M., Perrot, M., & Duchesnay, E. (2011). Scikit-learn: Machine Learning in Python. *Journal of Machine Learning Research*, *12*, 2825-2830.

Perez, K., Ciotlos, S., McGirr, J., Limbad, C., Doi, R., Nederveen, J. P., Nilsson, M. I., Winer, D. A., Evans, W., Tarnopolsky, M., Campisi, J., & Melov, S. (2022). Single nuclei profiling identifies cell specific markers of skeletal muscle aging, frailty, and senescence. *Aging (Albany NY)*, *14*(23), 9393-9422. https://doi.org/10.18632/aging.204435

Reily, C., Stewart, T. J., Renfrow, M. B., & Novak, J. (2019). Glycosylation in health and disease. *Nat Rev Nephrol*, *15*(6), 346-366. https://doi.org/10.1038/s41581-019-0129-4

Rousseeuw, P. (1987). Silhouettes: a Graphical Aid to the Interpretation and Validation of Cluster Analysis. *Journal of Computational and Applied Mathematics*, *20*, 53-65.

Schjoldager, K. T., Narimatsu, Y., Joshi, H. J., & Clausen, H. (2020). Global view of human protein glycosylation pathways and functions. *Nat Rev Mol Cell Biol*, *21*(12), 729-749. https://doi.org/10.1038/s41580-020-00294-x

Segal, E., Shapira, M., Regev, A., Pe'er, D., Botstein, D., Koller, D., & Friedman, N. (2003). Module networks: identifying regulatory modules and their condition-specific regulators from gene expression data. *Nat Genet*, *34*(2), 166-176. https://doi.org/10.1038/ng1165

Tabula Muris, C. (2020). A single-cell transcriptomic atlas characterizes ageing tissues in the mouse. *Nature*, *583*(7817), 590-595. https://doi.org/10.1038/s41586-020-2496-1

Tabula Sapiens, C., Jones, R. C., Karkanias, J., Krasnow, M. A., Pisco, A. O., Quake, S. R., Salzman, J., Yosef, N., Bulthaup, B., Brown, P., Harper, W., Hemenez, M., Ponnusamy, R., Salehi, A., Sanagavarapu, B. A., Spallino, E., Aaron, K. A., Concepcion, W., Gardner, J. M., . . . Wyss-Coray, T. (2022). The Tabula Sapiens: A multiple-organ, single-cell transcriptomic atlas of humans. *Science*, *376*(6594), eabl4896. https://doi.org/10.1126/science.abl4896

Tian, Y., Carpp, L. N., Miller, H. E. R., Zager, M., Newell, E. W., & Gottardo, R. (2022). Single-cell immunology of SARS-CoV-2 infection. *Nat Biotechnol*, *40*(1), 30-41. https://doi.org/10.1038/s41587-021-01131-y

Varki, A. (2017). Biological roles of glycans. *Glycobiology*, *27*(1), 3-49. https://doi.org/10.1093/glycob/cww086

Wang, S., Sontag, E. D., & Lauffenburger, D. A. (2023). What cannot be seen correctly in 2D visualizations of single-cell 'omics data? *Cell Syst*, *14*(9), 723-731. https://doi.org/10.1016/j.cels.2023.07.002

Wolf, F. A., Angerer, P., & Theis, F. J. (2018). SCANPY: large-scale single-cell gene expression data analysis. *Genome Biol*, *19*(1), 15. https://doi.org/10.1186/s13059-017-1382-0

Yang, J. M., Byrd, J. C., Siddiki, B. B., Chung, Y. S., Okuno, M., Sowa, M., Kim, Y. S., Matta, K. L., & Brockhausen, I. (1994). Alterations of O-glycan biosynthesis in human colon cancer tissues. *Glycobiology*, *4*(6), 873-884. https://doi.org/10.1093/glycob/4.6.873

Yang, S., Corbett, S. E., Koga, Y., Wang, Z., Johnson, W. E., Yajima, M., & Campbell, J. D. (2020). Decontamination of ambient RNA in single-cell RNA-seq with DecontX. *Genome Biol*, *21*(1), 57. https://doi.org/10.1186/s13059-020-1950-6

Figure Labels

Figure 1. Transcriptomic analysis of glycogenes at single cell level. (A) Summary of data preprocessing and analyses of Tabula Sapiens (TS) data (see Methods for details). (B) Number of glycogenes with RNA count > 0. Each dot represents a cell. Dark line represents the median value. The shaded areas show contour of percentiles at 10 percent increments from the median, spanning 0th to 100th percentile. The data collection results in a shoulder at ~65,000 UMI counts/cell corresponding to ~165 glycogenes. (C) A positive correlation is observed between the number of detected glycogenes vs. other protein coding (PC) genes. The face color represents the UMI depth. (D) Distribution of PC and glycogene expressions in terms of the number of expressing cells (*i.e.*, cells with nonzero RNA count for the gene). Glycogenes are generally more commonly expressed in the TS cells than other PC genes. (E) Distribution of single cell expression of glycogenes. Glycogenes are grouped based on their biological functions as defined in the GlycoEnzOnto (see **Supplementary Table S2**). 'Transporters and Regulators' are generally more broadly expressed compared to other glycogenes including glycosyltransferases. (F) Distribution of single cell expression of glycosyltransferases in Core, Extension and Terminal groups (see **Supplementary Table S3**). Core enzyme expression is higher compared to extension and terminal modifiers (G-H) UMAP visualization of scVI latent embedding of glycogene expression in epithelial cells and blood tissue.

Figure 2. Differential expression (DE) analysis of glycopathway in epithelial cells. (A) "GSL (glycosphingolipids) diversify" pathway including the gene set B4GALNT1, B3GALT4, B3GNT5, B3GALT5, B4GALT1, B3GALNT1 and A4GALT, is used to illustrate the calculation scheme. Here, mean pathway gene expression in each tissue is first calculated from the zero-inflated single-cell data. Log-fold change (LogFC) expression is then determined, and this is presented using dots where a thicker red (blue) linewidth represents higher (lower) levels of the pathway expression in a given tissue with respect to all other tissue. The face color of the dot (greyscale) represents the mean expression of the glycopathway among the cells in a specific tissue. (B) DE of glycopathways is presented for selected Core, Extension and Terminal pathways for epithelial cells. The greyscale heatmap in the last column presents the mean glycopathway expression among all epithelial cells. As an example, O-GlcNAc related genes (OGA, OGT) are highly expressed across tissue. Among the tissue, this is most highly expressed in the liver compared to kidney and large intestine. In contrast the GSL diversity genes are higher in eye and trachea compared to other tissue.

Figure 3. Enrichment-Depletion (ED) analysis of glycopathway in epithelial cells. (A) GSL (glycosphingolipids) diversify pathway is used to illustrate calculation scheme. ED analysis was performed by constructing the contingency table. The size of the dot represents the p-value of the Fisher exact test for significance, while the face color gives the sign of the log-odds ratio (logOR, blue: negative logFC and red: positive logFC). A negative logOR represents a depletion, while a positive logOR represents an enrichment of glycopathway in a tissue with respect to all other tissue with the same pathway. (B) ED of glycopathways in Core, Extension and Terminal groups for epithelial cells. The last column presents the fraction of expressing cells for each glycopathway among all epithelial cells using greyscale heatmap. This allows evaluation of how prevalent a given pathway is in epithelial cells compared to other pathways.

Figure 4. Glycosylation Transcription Factor Analysis. (A) Hiearchical clustering of glycogenes based on (logarithm) NMIs of TF-glycogene. (B) Silhouette analysis of *k*-means clustering. The maximum silhouette score at $k = 2$ suggests the existence of two transcriptional regulatory modules (TRMs) in the TS dataset. (C) Enrichment analysis of TRMs for glycopathways. The glycopathway groups marked in blue have

statistically significant odds ratio (two-sided Fisher exact test, α=0.05 with Bonferonni correction). (D) Sizes of shared and distinct transcription factors associated with glycogene regulatory clusters (see **Suppl. Table S5** for TFs).

Figure 1

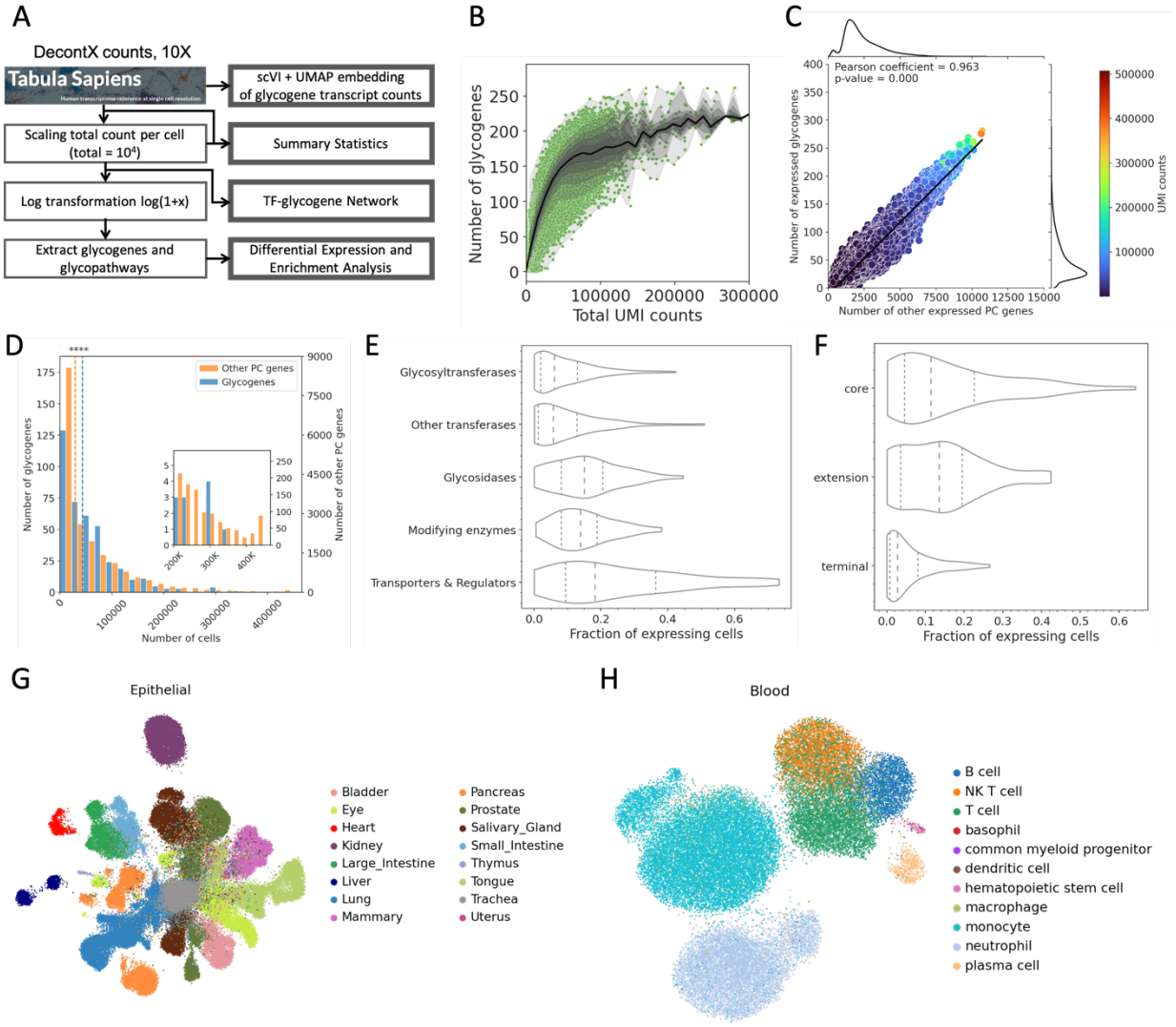
A
DecontX counts, 10X
Tabula Sapiens
scVI + UMAP embedding of glycogene transcript counts
Scaling total count per cell (total = 10⁴)
Summary Statistics
Log transformation log(1+x)
TF-glycogene Network
Extract glycogenes and glycopathways
Differential Expression and Enrichment Analysis
B
Number of glycogenes
Total UMI counts
C
Pearson coefficient = 0.963
p-value = 0.000
Number of expressed glycogenes
Number of other expressed PC genes
UMI counts
D
Other PC genes
Glycogenes
Number of glycogenes
Number of other PC genes
Number of cells
E
Glycosyltransferases
Other transferases
Glycosidases
Modifying enzymes
Transporters & Regulators
Fraction of expressing cells
F
core
extension
terminal
Fraction of expressing cells
G
Epithelial
Bladder
Eye
Heart
Kidney
Large_Intestine
Liver
Lung
Mammary
Pancreas
Prostate
Salivary_Gland
Small_Intestine
Thymus
Tongue
Trachea
Uterus
H
Blood
B cell
NK T cell
T cell
basophil
common myeloid progenitor
dendritic cell
hematopoietic stem cell
macrophage
monocyte
neutrophil
plasma cell

Figure 2

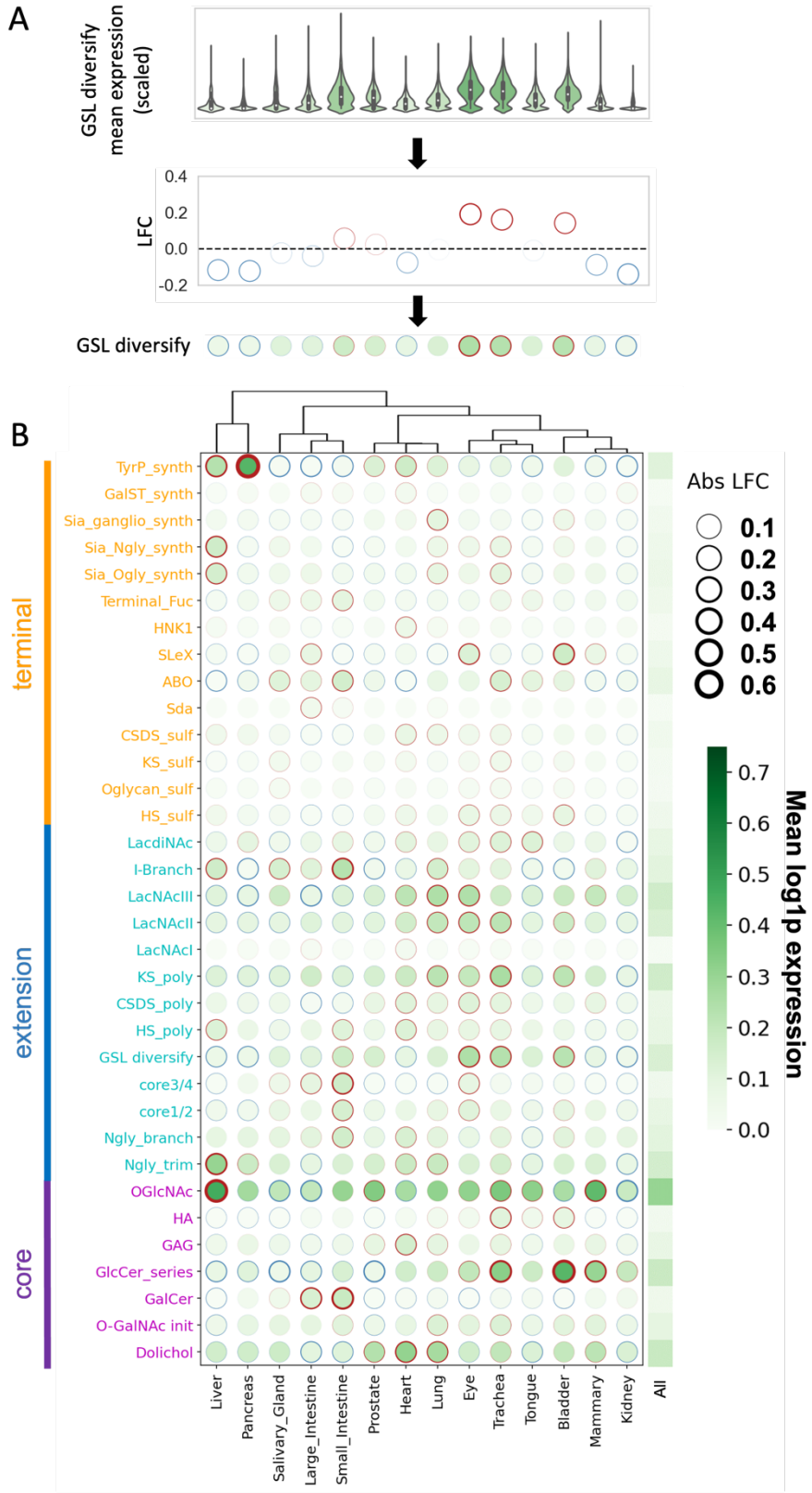
A
GSL diversify mean expression (scaled)
LFC
0.4
0.2
0.0
-0.2
GSL diversify
B
terminal
extension
core
TyrP_synth
GalST_synth
Sia_ganglio_synth
Sia_Ngly_synth
Sia_Ogly_synth
Terminal_Fuc
HNK1
SLeX
ABO
Sda
CSDS_sulf
KS_sulf
Oglycan_sulf
HS_sulf
LacdiNAc
I-Branch
LacNAcIII
LacNAcII
LacNAcI
KS_poly
CSDS_poly
HS_poly
GSL diversify
core3/4
core1/2
Ngly_branch
Ngly_trim
OGlcNAc
HA
GAG
GlcCer_series
GalCer
O-GalNAc init
Dolichol
Liver
Pancreas
Salivary_Gland
Large_Intestine
Small_Intestine
Prostate
Heart
Lung
Eye
Trachea
Tongue
Bladder
Mammary
Kidney
All
Abs LFC
0.1
0.2
0.3
0.4
0.5
0.6
Mean log1p expression
0.7
0.6
0.5
0.4
0.3
0.2
0.1
0.0

Figure 3

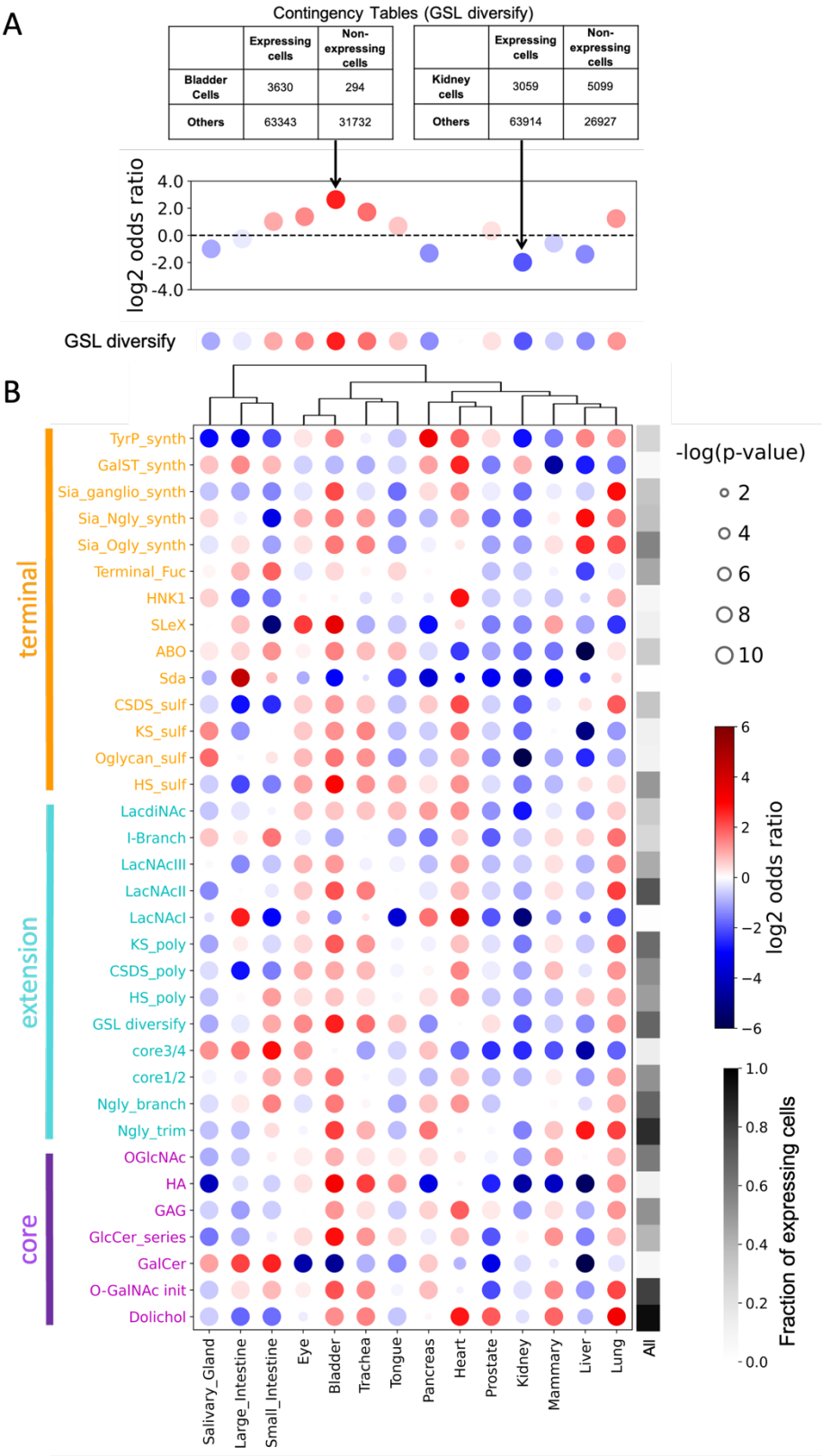
A
Contingency Tables (GSL diversify)
Expressing cells
Non-expressing cells
Bladder Cells
3630
294
Others
63343
31732
Expressing cells
Non-expressing cells
Kidney cells
3059
5099
Others
63914
26927
log2 odds ratio
4.0
2.0
0.0
-2.0
-4.0
GSL diversify
B
terminal
extension
core
TyrP_synth
GalST_synth
Sia_ganglio_synth
Sia_Ngly_synth
Sia_Ogly_synth
Terminal_Fuc
HNK1
SLeX
ABO
Sda
CSDS_sulf
KS_sulf
Oglycan_sulf
HS_sulf
LacdiNAc
I-Branch
LacNAcIII
LacNAcII
LacNAcI
KS_poly
CSDS_poly
HS_poly
GSL diversify
core3/4
core1/2
Ngly_branch
Ngly_trim
OGlcNAc
HA
GAG
GlcCer_series
GalCer
O-GalNAc init
Dolichol
Salivary_Gland
Large_Intestine
Small_Intestine
Eye
Bladder
Trachea
Tongue
Pancreas
Heart
Prostate
Kidney
Mammary
Liver
Lung
All
-log(p-value)
2
4
6
8
10
log2 odds ratio
6
4
2
0
−2
−4
−6
Fraction of expressing cells
1.0
0.8
0.6
0.4
0.2
0.0

Figure 4

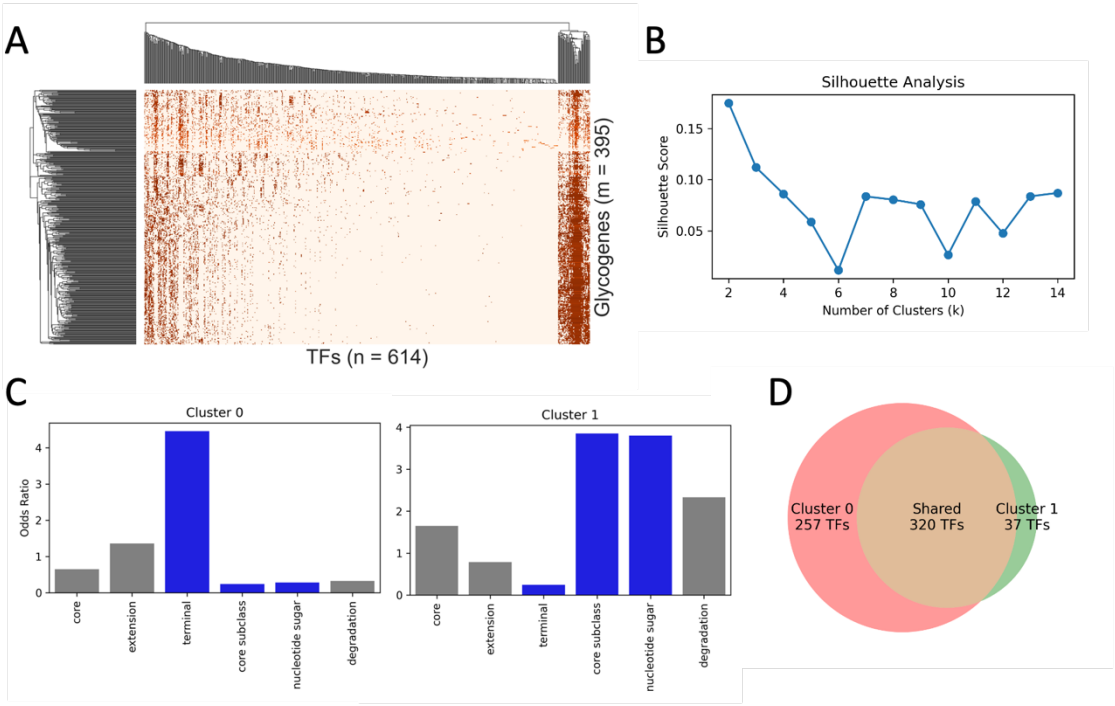
A
Glycogenes (m = 395)
TFs (n = 614)
B
Silhouette Analysis
Silhouette Score
Number of Clusters (k)
C
Cluster 0
Cluster 1
Odds Ratio
core
extension
terminal
core subclass
nucleotide sugar
degradation
D
Cluster 0
257 TFs
Shared
320 TFs
Cluster 1
37 TFs